Applied Catalysis B: Environmental 321 (2023) 122008

Contents lists available at ScienceDirect

Applied Catalysis B: Environmental

journal homepage: www.elsevier.com/locate/apcatb

A new and highly efficient co-catalyst Zn-Ni_5P_4 for photocatalytic H_2 evolution with the reduced capacitance via Zn doping

Li Luo, Jinfeng Tian, Wenfeng Hu, Peng Han, Wei Wang, Baojun Ma *

State Key Laboratory of High-efficiency Coal Utilization and Green Chemical Engineering, College of Chemistry and Chemical Engineering, Ningxia University, Yinchuan 750021, People's Republic of China

ARTICLE INFO

Keywords:
Zn-Ni_5P_4
Capacitance catalysis
Negative effect
Non-noble metal co-catalyst
Hydrogen production

ABSTRACT

Non-noble metal co-catalysts for hydrogen production have capacitance characterization, which can store photo-excited electrons from semiconductor and show capacitance catalysis. However, the overlarge capacitance of co-catalysts constrains prompt release of electrons. Here, we reported a new and highly efficient co-catalyst Zn-Ni_5P_4 via evenly doping Zn in Ni_5P_4. Loading Zn-Ni_5P_4 on CdS, the photocatalyst Zn-Ni_5P_4/CdS shows an ultrahigh activity of 8969 μmol/g/h, which is 2.4 times of Ni_5P_4/CdS (3668 μmol/g/h). More interestingly, by the Pt loading on the surface of Ni_5P_4, the (Pt/Ni_5P_4)/CdS shows only 1.3 times of Ni_5P_4/CdS. Zn doping in Ni_5P_4 reduces the capacitance by 140 mF/g and electrochemical impedance, which benefits the release of photo-excited electrons. Moreover, the reduced overpotential and the increased specific surface area also account for the enhanced co-catalytic performance of Zn-Ni_5P_4. This paper presents an effective and low-cost method to inhibit negative effect of capacitance catalysis of non noble co-catalysts.

1. Introduction

With the sustainable advancement of human society, efficient, clean and renewable hydrogen energy has attracted increasing attention. Photocatalytic water splitting to produce hydrogen on semiconductors utilizing solar energy is an ideal but challenging technology on account of their extremely low efficiency [1–9]. Co-catalysts modification is an effective mean to improve photocatalytic activities of semiconductors. Transition metal-based compounds co-catalysts (phosphides [10–12], carbides [13–15], sulfides [16,17] and nitrides [18,19]) have extensively used in photocatalytic water splitting due to their abundant reserve, low cost, and admirable catalytic performance. Nevertheless, the intrinsic essence of transition metal-based non-noble metal co-catalysts for hydrogen evolution need to be deeply illustrated and their co-catalytic performances have great spaces to improve.

Our group devotes to the research of the non-noble metal co-catalysts. Recently, we proposed a new concept of "capacitance catalysis" [14] in the study of Mo_2C co-catalysts. In the photocatalytic process, Mo_2C with larger capacitance can store more electrons (positive effect) of CdS and promote the separation of photo-excited electrons and holes to enhance the co-catalytic efficiency. Unfortunately, overlarge capacitance confines the release of electrons (negative effect) trapped by Mo_2C, inhibiting the co-catalytic ability of Mo_2C. Only with proper capacitance, Mo_2C shows the best co-catalytic hydrogen production performance balancing the store and releasing of the photo-excited electrons.

Further, we put forwarded an effective measure to weaken the negative effect of the co-catalyst capacitance. That is, loading noble metals on non-noble metal co-catalysts to construct composite co-catalysts. The noble metal decreases the capacitance of non-noble metal co-catalyst, accelerates the transport of electrons and act as the catalytic active centers, thus effectively inhibiting the negative influence of capacitance. For instance, Pt/Mo_2C [14], Ru/WC [20], Pt/Mo_2N [19] and Pd/MoP [11] composite co-catalysts loading on host catalyst CdS, the hydrogen production activities of are 1.46 times, 2.1 times, 1.3 times and 1.6 times of corresponding alone non-noble metals loaded on CdS, respectively. Although the content of non-noble metals in the above studies is very low, the introduction of noble metals makes such catalysts still difficult to achieve large-scale applications.

Therefore, it is crucial to develop photocatalysts with high activity and low cost for industrialization advancement. Several years ago, we accidentally prepared W doped WC co-catalyst [21]. The presence of metal W reduces the capacitance of WC and improves its co-catalytic performance for photocatalytic H_2 evolution. Therefore, it is worth

* Corresponding author.
E-mail address: bjma@nxu.edu.cn (B. Ma).

https://doi.org/10.1016/j.apcatb.2022.122008
Received 20 July 2022; Received in revised form 14 September 2022; Accepted 18 September 2022
Available online 20 September 2022
0926-3373/© 2022 Elsevier B.V. All rights reserved.

studying that the capacitance of the cheap non-noble metal co-catalyst and its negative effect can be reduced by doping transition metals or transition metal compounds instead of noble metals.

The transition metal compound Ni_5P_4 is a high-performance electrocatalyts and photocatalysts [22–26]. Here, we design Zn-doped Ni_5P_4 composite co-catalyst using Zn doping instead of noble metals loading. The photocatalyst Zn-Ni_5P_4/CdS exhibits an ultra-high hydrogen production activity of 8969 μmol/g/h, which is 2.4 times that of Ni_5P_4/CdS. The Zn doping reduces the capacitance of Ni_5P_4 from 680 to 540 mF/g and improves electrons transport, thereby weakening the negative effect of capacitance and benefiting the release of photo-excited electrons. The report opens up a new avenue to constrain the negative influence of co-catalyst capacitance by doping transition metal.

2. Experimental section

2.1. Preparation of catalysts

Except H_2PtCl_6•6 H_2O, which was purchased from Shanghai Aladdin, other reagents were purchased from Sinopharm Chemical Reagent Co., Ltd. (Beijing, China). All reagents are analytical grade and are directly used in experiments.

2.2. Preparation of Zn-Ni_5P_4

Zn-Ni_5P_4 was prepared by a two-step hydrothermal-calcination process. In detail, 0.6239 g of nickel chloride hexahydrate, 0.1944 g of ammonium fluoride, 0.7884 g of urea and 0.0885 g of zinc nitrate hexahydrate were dissolved in 70 mL of deionized water. After stirring for 20 min, the mixed solution was transferred to a 100 mL Teflon-lined autoclave and then hydrothermal reaction at 120 °C for 6 h. Then the product was centrifuged for several times with deionized water and absolute ethanol, and dried for 12 h to obtain the precursor. Finally, 1.0 g of $NaH_2PO_2{\cdot}H_2O$ and 0.1 g of precursor were placed in the upstream and downstream of a tubular furnace and calcined in a 100 mL/min of N_2 atmosphere at 350 °C for 2 h. The obtained sample is labeled 8%Zn-Ni_5P_4. Using the same method as above, adding different amount of zinc nitrate hexahydrate obtained 3%, 5%, 12%, 16%Zn doped Ni_5P_4. The Fe-Ni_5P_4, Co-Ni_5P_4, Cu-Ni_5P_4 were synthesized by using ferric nitrate nonahydrate, cobalt nitrate hexahydrate, and cupric Sulfate Pentahydrate instead of nickel chloride hexahydrate, respectively. Ni_5P_4 was prepared by the same method without adding zinc nitrate hexahydrate.

2.3. Preparation of Pt/Zn-Ni_5P_4 and Pt/Ni_5P_4

0.2 g of Zn-Ni_5P_4 and a certain volume of H_2PtCl_6•6 H_2O solution (1.0 mg/mL) were added to 30 mL of deionized water, and then heated to dryness at 80 °C. Next, the dried samples were put into a tube furnace and reduced at 300 °Cfor 1 h in a H_2 atmosphere of 50 mL/min to obtain xPt/Zn-Ni_5P_4 (x = 0.1%, 0.5%, 1.0%). The preparation process of Pt/Ni_5P_4 is similar to that of Pt/Zn-Ni_5P_4.

2.4. Preparation of Zn-Ni_5P_4/CdS, Ni_5P_4/CdS, (Pt/Zn-Ni_5P_4) /CdS and (Pt/Ni_5P_4)/CdS

Preparation of Zn-Ni_5P_4/CdS by a simple co-precipitation method. First, the Zn-Ni_5P_4 of different mass (0.0263 g, 0.0556 g, 0.0882 g, 0.125 g, 0.1667 g, 0.2692 g, 0.5 g) were uniformly dispersed in 25 mL of 0.14 mol/L cadmium nitrate solution, respectively. Subsequently, 30 mL of 0.14 mol/L sodium sulfide solution was dropped into the above solution and mechanically stirred for 1 h. After the mixtures were aged for 8 h, the precipitates were washed 6 times and dried at 60 °C to obtain the samples xZn-Ni_5P_4/CdS. (Here, x are the loading amounts of Zn-Ni_5P_4, x = 5%, 10%, 15%, 20%, 25%, 35%, 50%). In addition, Zn-Ni_5P_4 was replaced by Ni_5P_4, Pt/Ni_5P_4 and Pt/Zn-Ni_5P_4, respectively, and Ni_5P_4/CdS, (Pt/Ni_5P_4)/CdS and (Pt/Zn-Ni_5P_4)/CdS) were prepared by the same process as above.

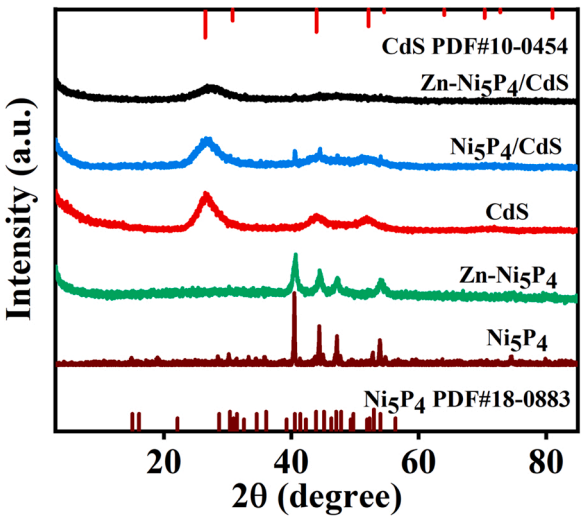

Fig. 1. The XRD patterns of different catalysts. The loading amounts of Ni_5P_4 in Ni_5P_4/CdS and Zn-Ni_5P_4 in Zn-Ni_5P_4/CdS are both 20%, and the doping amount of Zn in Zn-Ni_5P_4 is 8%.

2.5. Characterization

The XRD patterns, specific surface areas (SSA) and ultraviolet/visible diffuse reflectance spectra (UV/vis DRS) of the co-catalysts and composite photocatalysts were obtained by X-ray diffractometer (D8 ADVANCE A25), physical adsorption apparatus (ASAP 2460) and UH4150 spectrophotometer, respectively. The morphologies and structures of catalysts were characterized by SU8020 (USA) field emission scanning electron microscope (SEM) and FEI Tecnai G2 F30 (USA) transmission electron microscope (TEM), respectively. Elements and valences information on composite photocatalyst surface were measured with a Thermo Escalab 250Xi X-ray photoelectron spectroscopy (XPS) instrument. The surface photovoltage (SPV) signals of photocatalysts were tested via a lock-in amplifier (SR830), and the monochromatic light that excited the SPV signals was obtained via a 500 W xenon lamp (CHF-XM-500 W) and a grating monochromator (Omni-3007).

2.6. Photocatalytic water splitting for hydrogen production

The catalytic performance of the samples was evaluated by photocatalytic water splitting for hydrogen production activity tests. Specifically, 0.1 g of the photocatalyst was added to a lactic acid aqueous solution (containing 90 mL of H_2O and 10 mL of lactic acid), and the catalyst was uniformly dispersed by sonication for 10 min. Before the reaction, the air in the hydrogen-generating device was exhausted by a vacuum pump. Immediately afterwards, a PLS-SXE300/300UV xenon lamp (Perfect, China) was used as a visible light source (ultraviolet light was filtered by a 420 nm filter) to illuminate the reactor solution for 1 h. After the reaction was completed, the amount of hydrogen produced was detected by a GC 7900 gas chromatography and argon as the carrier gas (Shanghai Tianmei Scientific Instrument Co., Ltd.).

2.7. Photoelectrochemical experiments

The cyclic voltammetry (CV), linear sweep voltammetry (LSV) curves, electrochemical impedance spectroscopy (EIS) and transient photocurrent responses (TPR) were measured on a workstation of CHI 760E at room temperature. Na_2SO_4 (0.5 mol/L) was used as electrolyte to performance all photoelectrochemical characterizations. The LSV, EIS

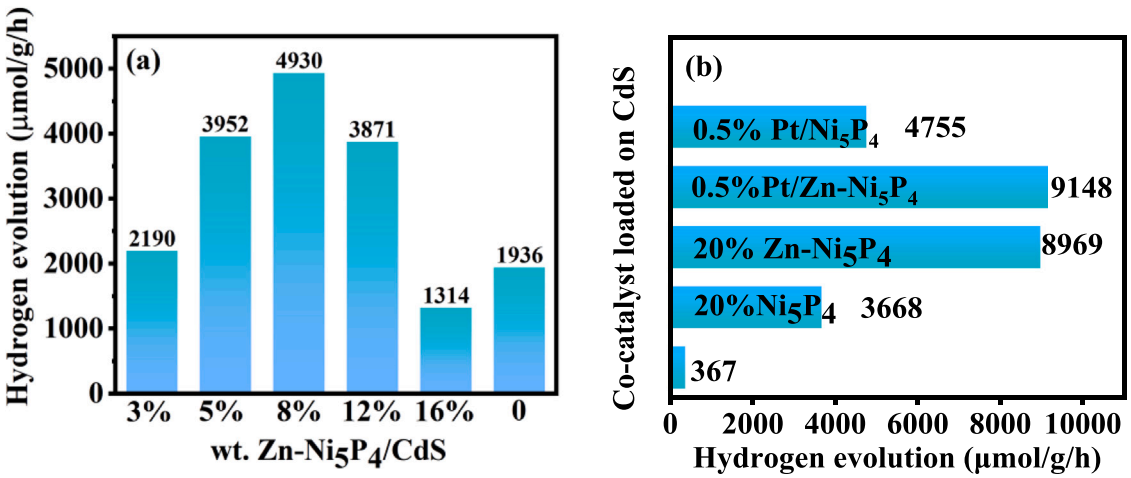

Fig. 2. (a) Hydrogen production activity of Ni_5P_4 with different Zn doping amounts loaded on CdS, and the loading amount of Zn-Ni_5P_4 are 3%. (b) The photocatalytic H_2 evolution on CdS with Pt load on co-catalysts, the loading amounts of Pt in (Pt/Ni_5P_4)/CdS and Zn-Ni_5P_4/CdS are 0.5%, the loading amounts of Ni_5P_4 in Ni_5P_4/CdS and (Pt/Ni_5P_4)/CdS is 20% and 19.5%, respectively, that of Zn-Ni_5P_4 in (Pt/Zn-Ni_5P_4)/CdS and Zn-Ni_5P_4/CdS is 19.5% and 20%, respectively, and the doping amount of Zn in Zn-Ni_5P_4 is 8%.

and TPR tests were performed with the catalyst-coated FTO as the working electrode, and the working electrode for the CV test was nickel foam. The saturated calomel electrode and platinum mesh were used as reference and counter electrode, respectively. The specific capacitance is calculated from the formula [27]:

$$C = \frac{\int IdV}{mk\Delta E}$$

(Where, C (mF/g), $\int IdV$, m (mg), k (V/s), ΔE (V) are specific capacitance, integral area of the CV curve, mass of sample coated on nickel

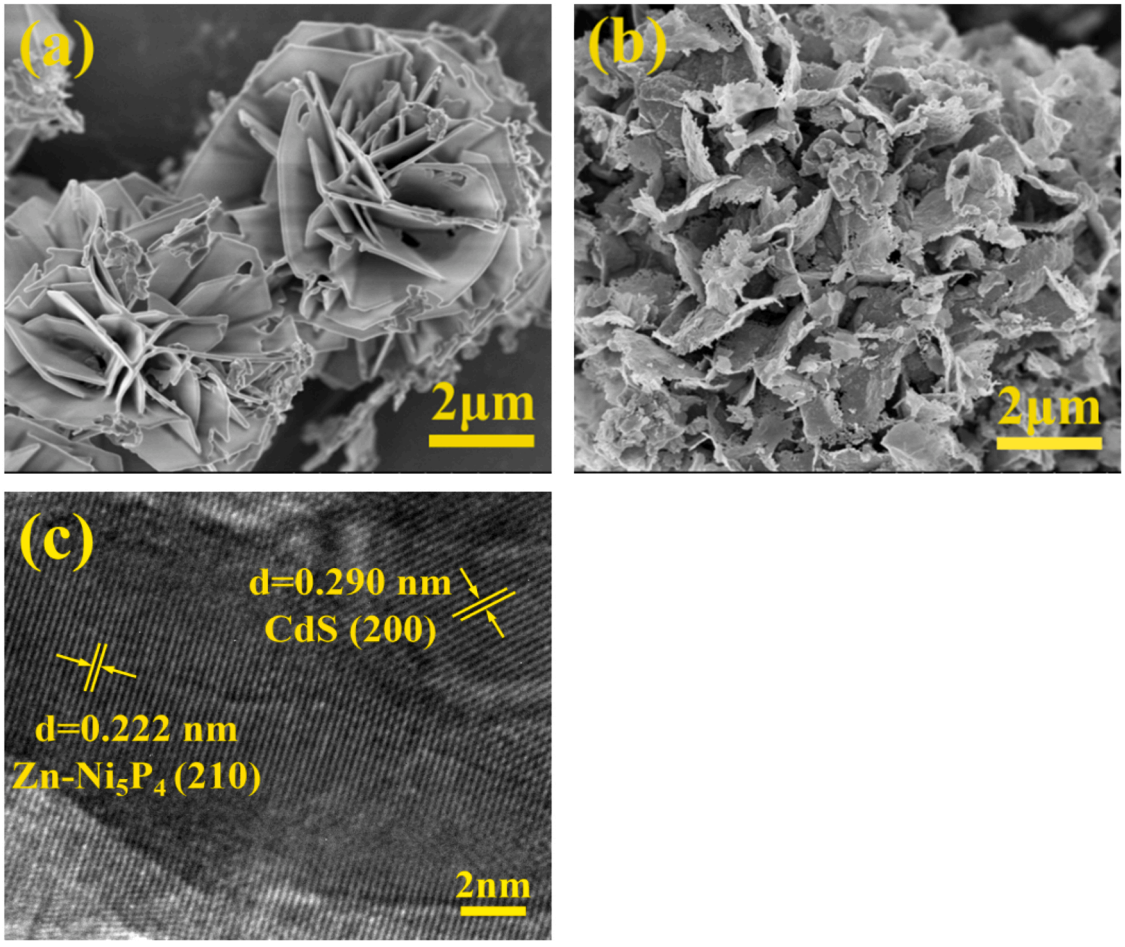

Fig. 3. The SEM images of Ni_5P_4 (a) and Zn-Ni_5P_4 (b), (c) The TEM images of Zn-Ni_5P_4/CdS. The loading amount of Zn-Ni_5P_4 in Zn-Ni_5P_4/CdS is 20%, and the doping amount of Zn in Zn-Ni_5P_4 is 8%.

Table 1
The specific surface areas (SSA) of different catalysts.

Catalysts	Ni_5P_4	Zn-Ni_5P_4	CdS	Ni_5P_4/CdS	Zn-Ni_5P_4/CdS
SSA (m^2/g)	4.50	57.90	31.95	75.55	94.51

foam, scan rate and potential window, respectively).

3. Results and discussion

3.1. The physical and chemical properties of catalysts

The crystal structures of catalysts (as shown in Fig. 1) were characterized by a the X-ray diffractometer. The characteristic diffraction peaks of Ni_5P_4 and CdS are consistent with those of the standard cards PDF#18–0883 and PDF#10–0454, respectively, indicating the successful preparation of co-catalyst Ni_5P_4 and host catalyst cubic phase CdS [28]. In addition, characteristic diffraction peaks of Ni_5P_4 can be observed in Ni_5P_4/CdS, demonstrating the successful synthesis of Ni_5P_4/CdS. Due to the low amount of Zn and evenly doping in Ni_5P_4, so the Zn-Ni_5P_4 shows the characteristic peaks similar to Ni_5P_4. Also, the characteristic peaks of Zn-Ni_5P_4/CdS are similar to those of Ni_5P_4/CdS.

We explore the co-catalytic performance of different transition metals (Fe, Co, Cu, Zn) doping in Ni_5P_4, the 3%Zn-Ni_5P_4/CdS has the highest catalytic activity for hydrogen evolution (as shown in Fig. S1a). Therefore, we use Zn-Ni_5P_4 as the co-catalyst to study the effect of Zn doping on the hydrogen production performance of the Ni_5P_4 co-catalyst. Fig. 2a shows the effect of different Zn doping amounts on the photocatalytic activity of Ni_5P_4/CdS. The Zn-Ni_5P_4/CdS with 8% Zn doping has optimal hydrogen production activity. Fig. S1b shows the effect of the loading amount of Zn-Ni_5P_4 on the photocatalytic activity of CdS and the optimal loading amount is 20%. Fig. 2b shows the hydrogen production activities of different co-catalysts loading on CdS, it is obvious that Zn-Ni_5P_4/CdS exhibits ultrahigh activities of 8969 μmol/g/h for H_2 evolution, which are 24.4 times and 2.4 times of CdS (367 μmol/g/h) and Ni_5P_4/CdS (3668 μmol/g/h), respectively, and the catalyst maintains good stability under continuous 20 h reaction (Fig. S2). When the noble metal Pt loaded on the surface of Ni_5P_4 to construct Pt/Ni_5P_4 composite co-catalyst, the activity of (0.5% Pt/Ni_5P_4)/CdS (4755 μmol/g/h) shows 1.3 times of Ni_5P_4/CdS, indicating the effective strategy of deposition noble metal on the non-noble metal co-catalyst surface. Interestingly, the activity of Zn-Ni_5P_4/CdS is 1.89 times and much higher of (Pt/Ni_5P_4)/CdS, demonstrating that Zn doping is more effective than Pt loading. Further, when the Pt is deposited on Zn-Ni_5P_4, the activity of (Pt/Zn-Ni_5P_4)/CdS almost equal to that of Zn-Ni_5P_4/CdS, suggesting Zn plays the role similar to Pt. The effect of Pt content on the CdS hydrogen production activity is shown in Fig. S1c, the optimal loading amount of Pt in (Pt/Ni_5P_4)/CdS and (Pt/Zn-Ni_5P_4)/CdS both are 0.5%.

The morphologies images of the co-catalysts were observed by SEM. Obviously, both Ni_5P_4 (Fig. 3a) and Zn-Ni_5P_4 (Fig. 3b) exhibit a carnation flower-like structure. After the doping of Zn, Zn-Ni_5P_4 still shows a flower-like structure, but the surfaces of the petals become rough, which means that the specific surface area becomes larger. Table 1 shows the specific surface areas (SSA) of different catalysts. The specific surface area of Ni_5P_4 is only 4.50 m^2/g, and Zn doping notably enlarges the specific surface area of Ni_5P_4 (up to 57.90 m^2/g). Compared with pure CdS, the SSA of the co-catalysts modified CdS are improved, and Zn-Ni_5P_4/CdS presents the highest SSA of 94.51 m^2/g. The larger specific surface area can provide more active sites for the photocatalytic hydrogen production reaction. Fig. 3c shows the TEM image of Zn-Ni_5P_4/CdS. The lattice fringes with interplanar spacing of 0.222 nm are assigned to the (210) plane of co-catalyst Zn-Ni_5P_4. The lattice fringes with an interplanar spacing of 0.290 nm are assigned to the (200) plane

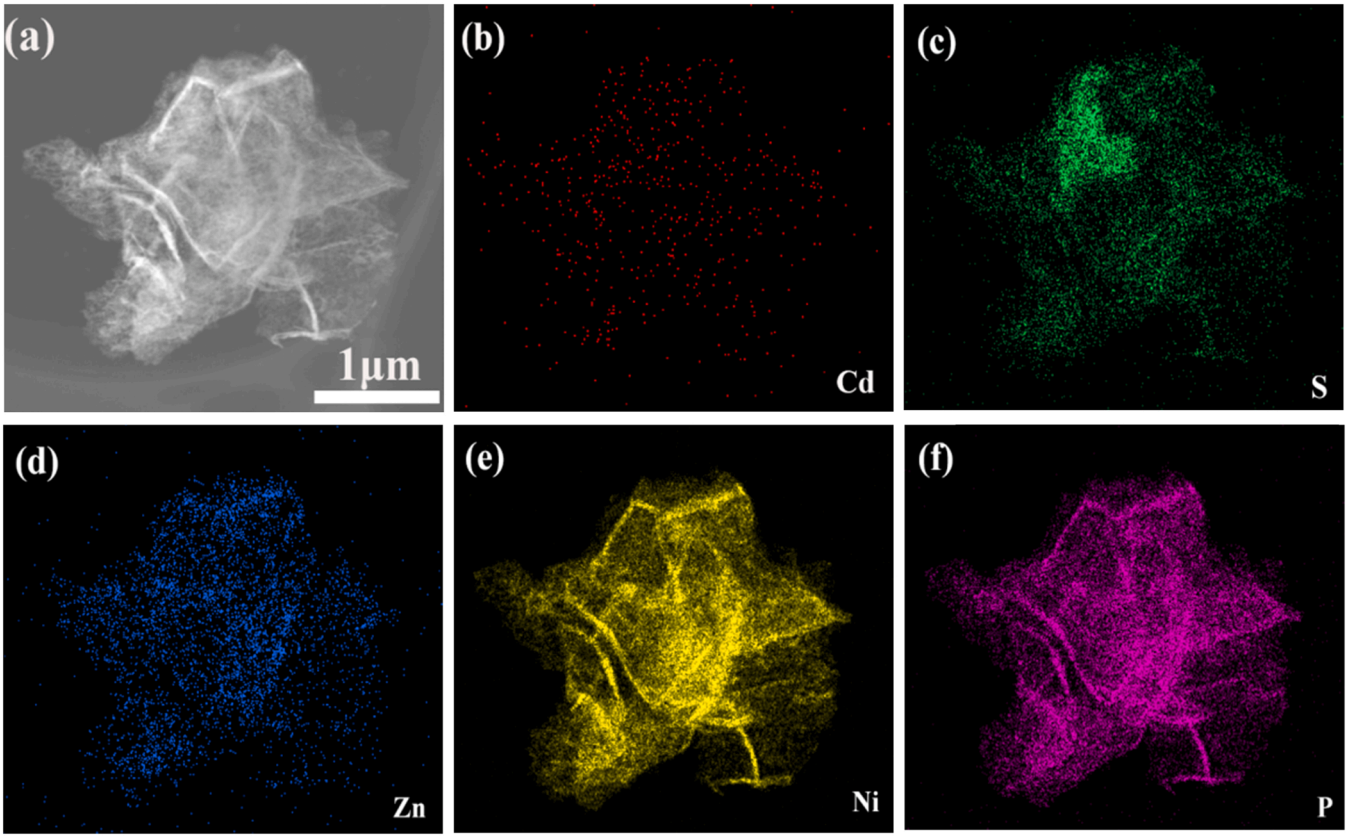

Fig. 4. The elemental mappings of Cd, S, Zn, Ni and P elements of Zn-Ni_5P_4/CdS. The loading amount of Zn-Ni_5P_4 in Zn-Ni_5P_4/CdS is 20%, and the doping amount of Zn in Zn-Ni_5P_4 is 8%.

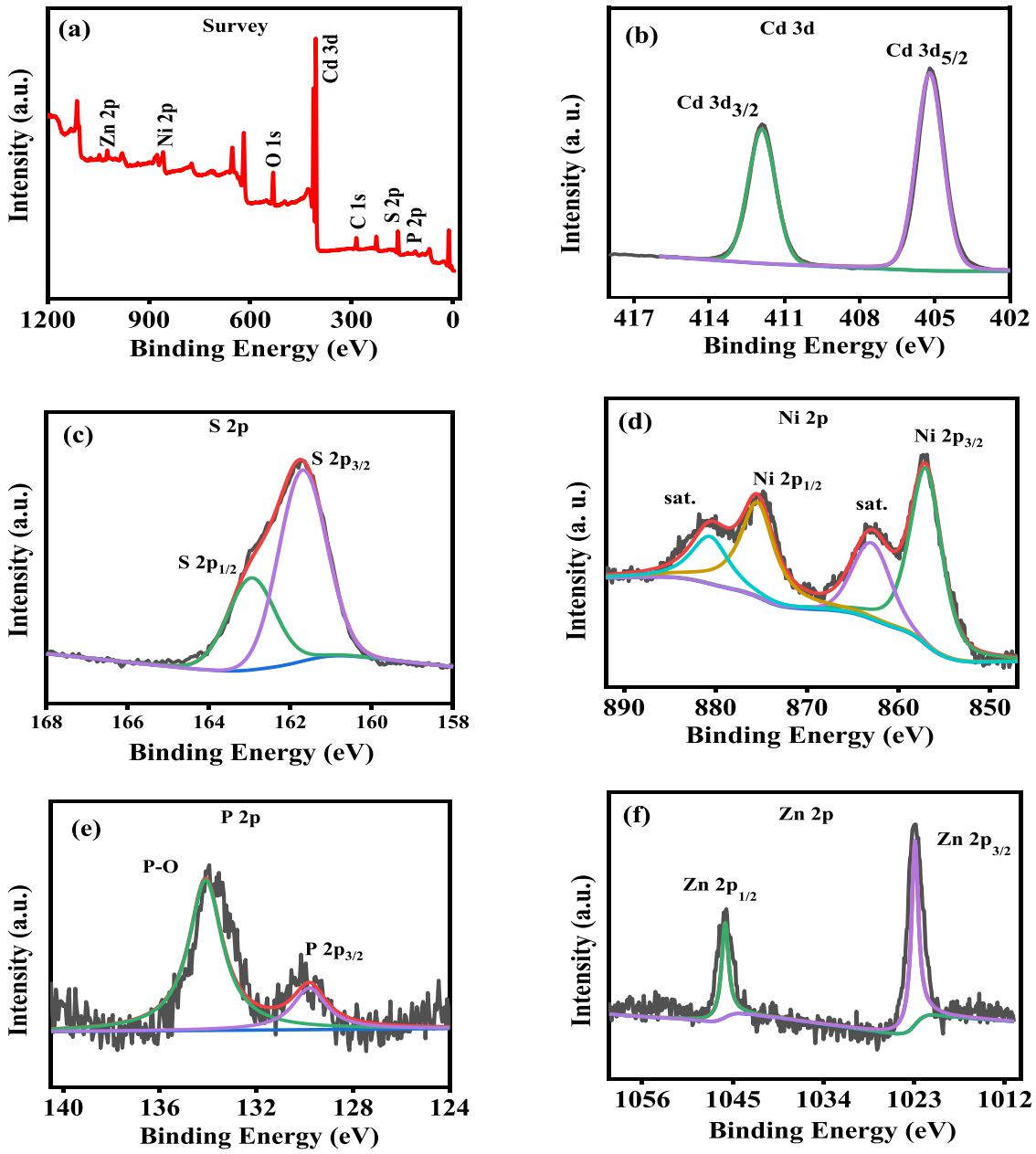

Fig. 5. The XPS spectra of Zn-Ni_5P_4/CdS. (a) XPS survey spectra, (b) Cd 3d, (c) S 2p, (d) Ni 2p, (e) P 2p and (f) Zn 2p. The loading amount of Zn-Ni_5P_4 in Zn-Ni_5P_4/CdS is 20%, and the doping amount of Zn in Zn-Ni_5P_4 is 8%.

of semiconductor CdS. The Zn-Ni_5P_4 and CdS are tightly bound together and which is favor of the electrons transport. The element mapping images (Fig. 4a-f) show the uniform distribution of Cd, S, Ni, P and Zn elements in Zn-Ni_5P_4/CdS.

The XPS (Fig. 5) is used to characterize the elements and valence states of Zn-Ni_5P_4/CdS surface. Fig. 5a confirms the existence of Cd, S, Zn, Ni, P and O elements. The presence of element O is the result of the catalyst being oxidized in air. The Cd 3d (Fig. 5b) high-resolution spectrum exhibits two peaks of $3d_{3/2}$ and $3d_{5/2}$ located at 411.9 and 405.2 eV [29], respectively, which can be assigned to Cd^{2+}. In the Fig. 5c, where the peaks of 161.7 eV and 162.95 eV are belonged to the S $2p_{3/2}$ and S $2p_{1/2}$ of S^{2-} [29], respectively. The binding energy at 875.6 eV and 857.1 eV (Fig. 5d) match with Ni $2p_{1/2}$ and Ni $2p_{3/2}$ of $Ni^{\delta+}$, in addition, the two peaks of 880.8 eV and 863 eV are corresponding to the satellite peaks [30]. In the Fig. 5e, the binding energy at 134.15 and 129.9 eV is attributed to the P-O bond and the metal-P bond of Zn-Ni_5P_4 [31], respectively. The Zn 2p high-resolution spectrum (Fig. 5f) displays the double peaks of 1022.8 and 1044.9 eV, which are attributed to Zn $2p_{3/2}$ and Zn $2p_{1/2}$ of Zn^{2+} in Zn species [31], respectively.

3.2. *The photoelectrochemical characterizations of different catalysts*

To elucidate the role of Zn doping, photoelectrochemical performancesof different catalysts were measured. Figs. 6a and 6b show the linear scanning voltammetry (LSV) curves of co-catalysts and relevant photocatalysts. Obviously, Zn doping reduces the over-potential (from −0.59 V to −0.57 V) of Ni_5P_4 (Fig. 6a) for hydrogen production. What's more, the Zn-Ni_5P_4/CdS shows the lowest of over-potential of hydrogen evolution (Fig. 6b), that means Zn-Ni_5P_4/CdS is the most favorable the hydrogen production reaction. Figs. 6c and 6d show the electrochemical impedance spectra (EIS) of different catalysts. Zn doped reduces Nyquist semicircle radius of Ni_5P_4, illustrating that the introduction of Zn reduces the interfacial charge transfer resistance of Ni_5P_4 (Fig. 6c).

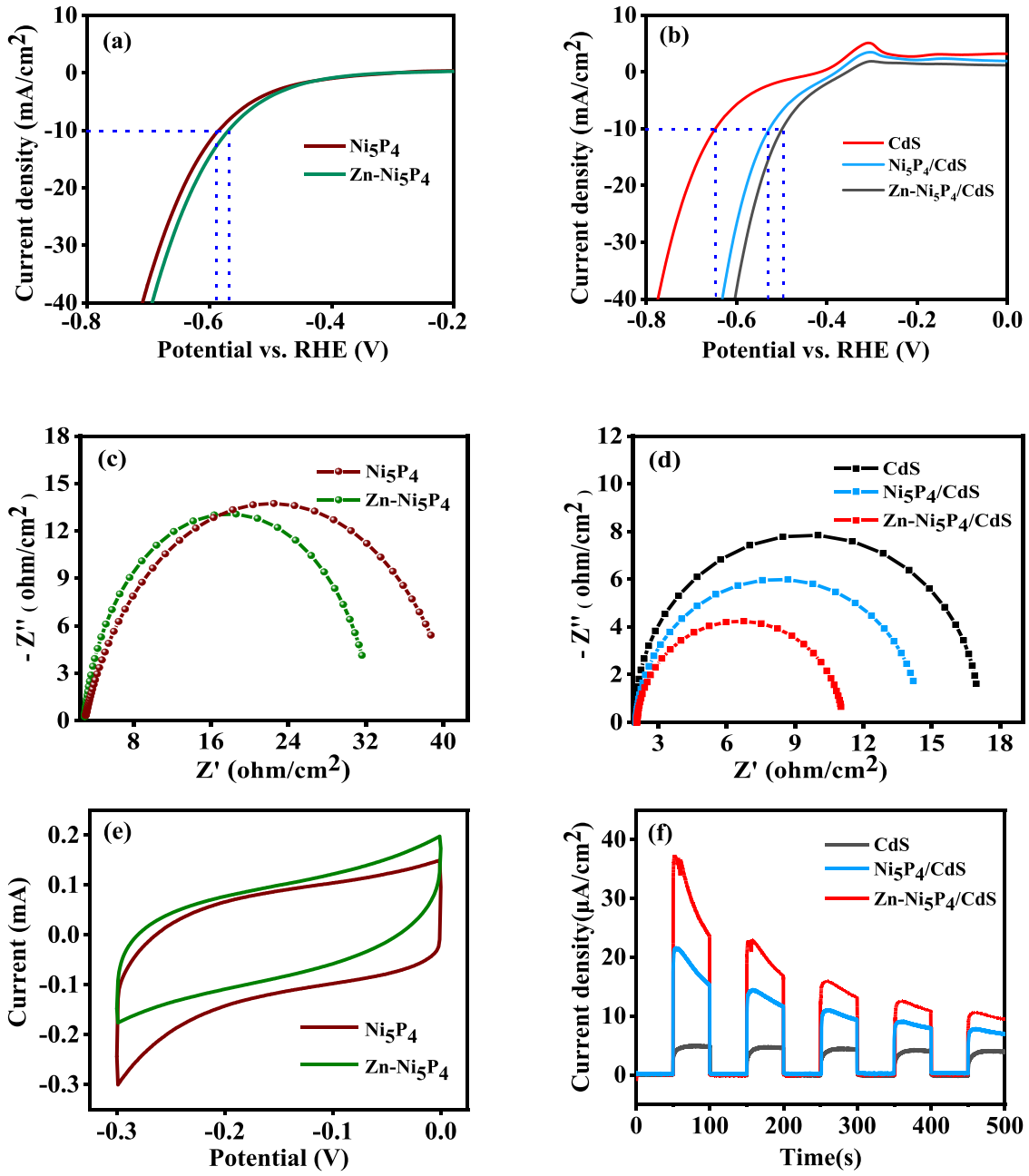

Fig. 6. (a. b) Linear sweep voltammetry curves, (c, d) Electrochemical impedance spectra, (e) Cyclic voltammetry curves at scan rate 50 mV/s and (f) Transient photocurrent responses. The loading amounts of Ni_5P_4 in Ni_5P_4/CdS and Zn-Ni_5P_4 in Zn-Ni_5P_4/CdS are both 20%, and the doping amount of Zn in Zn-Ni_5P_4 is 8%.

Table 2
The specific capacitance of co-catalysts.

Co-catalysts	Ni_5P_4	Zn-Ni_5P_4
Specific capacitance (mF/g)	680	540

Similarly, Zn-Ni_5P_4/CdS has the smallest interfacial charge transfer resistance, which is the most conducive to the transfer and separation of photo-generate electrons and holes for photocatalysis water splitting (Fig. 6d). Fig. 6e illustrates the cyclic voltammetry curves of different co-catalysts at scan rate of 50 mV/s. The specific capacitance of different catalysts was revealed in Table 2. The capacitance of 8%Zn-Ni_5P_4 (540 mF/g) was lower than that of Ni_5P_4 (680 mF/g). The Zn doping reduces the capacitance, which is favor of the electrons trapped in Ni_5P_4 fast transferring and releasing. Fig. 6 f shows the relationship between the photocurrent density and the illumination time of photocatalysts. CdS has the lowest photocurrent density, when Ni_5P_4 and Zn-Ni_5P_4 were loaded on CdS, the photocurrent densities of composite photocatalysts increase and Zn-Ni_5P_4 /CdS exhibits the highest photocurrent density, revealing Zn-Ni_5P_4 effective captures and transfers photo-excited electrons and dramatically enhances charges separation efficiency.

Fig. 7a shows the surface photovoltage spectra of different catalysts. The pure CdS has strong response in the range of 300–500 nm. Zn-Ni_5P_4/CdS exhibits the weakest SPV signal, followed by Ni_5P_4/CdS. The reduced SPV signal may be due to the short circuit phenomenon caused by the strong conductivity of the co-catalysts (Ni_5P_4 and Zn-Ni_5P_4), and the uniform distribution of photo-generated charges on CdS resulting from the uniform distribution of the co-catalyst on CdS [15]. Fig. 7a further demonstrates the superior electrical conductivity of Zn-Ni_5P_4. Fig. 7b shows the UV-Vis DRS of different catalysts. Both Ni_5P_4 and Zn-Ni_5P_4 exhibit wide spectra absorption, which is distinct from the

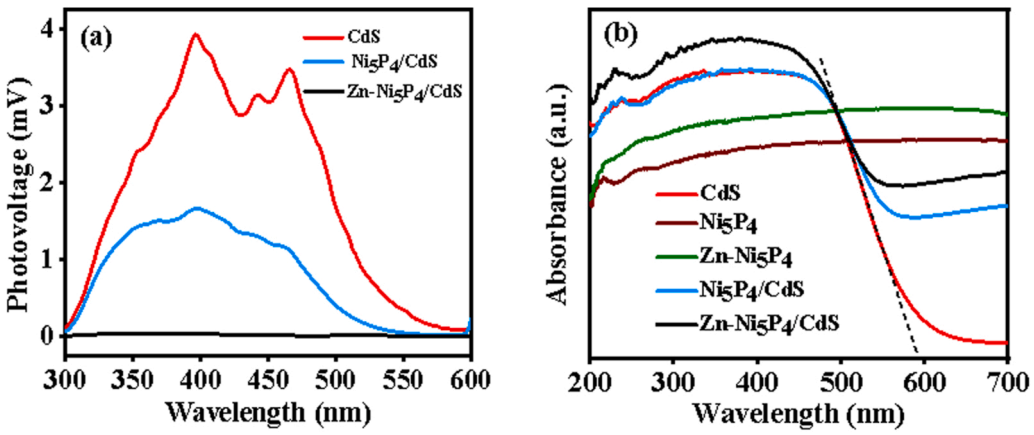

Fig. 7. (a) The SPV spectra, (b) the UV–vis DRS of different catalysts. The loading amounts of Ni_5P_4 in Ni_5P_4/CdS and Zn-Ni_5P_4 in Zn-Ni_5P_4/CdS are both 20%, and the doping amount of Zn in Zn-Ni_5P_4 is 8%.

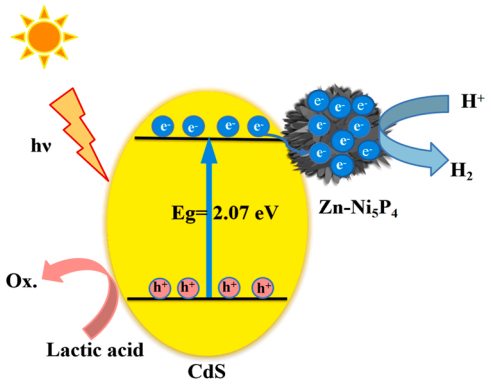

Scheme 1. The mechanism of photocatalytic water splitting of Zn-Ni_5P_4/CdS for hydrogen production.

semiconductor. The absorption band edge positions of all photocatalysts except co-catalysts are around 600 nm, corresponding to the band gap of CdS is 2.07 eV, and the co-catalysts loading enhances the tail light absorption intensity of CdS.

3.3. The mechanism of photocatalytic hydrogen production of Zn-Ni_5P_4/CdS

Scheme 1 exhibits the photocatalytic hydrogen production mechanism of Zn-Ni_5P_4/CdS. Under simulated sunlight irradiation, the semiconductor CdS is excited, and the photo-excited electrons transition from valence band to the conduction band. The holes in valence band undergo reduction reactions with the lactic acid (sacrificial agent) to reduce the recombination of photo-excited charges. At the same time, the electrons in conduction band are captured by the co-catalyst Zn-Ni_5P_4 and further undergo reduction reactions with H^+ to produce H_2. Duo to the super electrical conductivity of the co-catalyst Zn-Ni_5P_4, the photo-excited electrons in CdS can be rapidly migrated to Zn-Ni_5P_4. Most importantly, the reduced capacitance of Zn-Ni_5P_4, the electrons in Zn-Ni_5P_4 are more easily released into solution for H_2 evolution reaction, which vastly reduces the negative effective of capacitance catalysis. Additionally, Zn-Ni_5P_4/CdS has large specific surface area (rich active sites) and low overpotential for hydrogen production. Benefiting from the above advantages, the composite photocatalyst Zn-Ni_5P_4/CdS displays efficient photocatalytic H_2 evolution performance.

4. Conclusions

In short, we successfully reported a new and highly efficient Zn-Ni_5P_4 co-catalysts with carnation flower-like structure. The 20% Zn-Ni_5P_4/CdS shows high activity 8969 μmol/g/h for photocatalytic hydrogen production, which are 24.4 times and 2.4 times those of CdS and Ni_5P_4/CdS, respectively. However, the hydrogen H_2 evolution activity of (Pt/Zn-Ni_5P_4)/CdS is only 1.3 times that of Ni_5P_4/CdS. The introduction of Pt on Zn-Ni_5P_4 hardly improved the activity. The experiment results show that such non-noble metal Zn doping shows better effect than noble metal Pt loading. The Zn doping in Ni_5P_4 reduces the capacitance of Ni_5P_4 by 140 mF/g and electrochemical impedance, thereby suppressing the negative effect of the Ni_5P_4 capacitance catalysis. At the same time, Zn-Ni_5P_4 shows large specific surface area and low overpotential, which provides more active sites and accelerates the reaction kinetics of hydrogen evolution. So, the photocatalytic performance of Zn-Ni_5P_4/CdS is significantly improved. So far, the role of Zn doping has been elucidated. The report develops a new method of transition metals doping into non-noble metals co-catalysts to inhibit the negative effect of capacitance catalysis instead of noble metals loading.

CRediT authorship contribution statement

Li Luo: Investigation, Methodology, Formal analysis, Resources, Writing – original draft, Writing – review & editing. **Jinfeng Tian:** Formal analysis. **Wenfeng Hu:** Formal analysis. **Peng Han:** Data curation. **Wei Wang:** Validation, Supervision, Project administration. **Baojun Ma:** Supervision, Conceptualization, Funding acquisition, Methodology, Project administration.

Declaration of Competing Interest

The authors declare that they have no known competing financial interests or personal relationships that could have appeared to influence the work reported in this paper.

Data availability

I have shared the link to my date at the Attach File Step.

Acknowledgements

This work was supported by the Project of Science and Technology Innovation Team and Talent of Ningxia (2020CXTDLX08, 2021GKLRLX07), Project of Key Research Plan of Ningxia (2021BEE02017), the Natural Science Foundation of Ningxia

(2022AAC02015, 2022AAC03105), the National First-rate Discipline Construction Project of Ningxia (Chemical Engineering and Technology) and the National Natural Science Foundation of China (NSFC, 21862014).

Appendix A. Supporting information

Supplementary data associated with this article can be found in the online version at doi:10.1016/j.apcatb.2022.122008.

References

[1] J. Zhang, G. Chen, K. Müllen, X. Feng, Carbon-rich nanomaterials: fascinating hydrogen and oxygen electrocatalysts, Adv. Mater. 30 (2018) 1800528.
[2] J. Zhu, L. Hu, P. Zhao, L.Y.S. Lee, K.-Y. Wong, Recent advances in electrocatalytic hydrogen evolution using nanoparticles, Chem. Rev. 120 (2020) 851–918.
[3] X. Chen, S. Shen, L. Guo, S.S. Mao, Semiconductor-based photocatalytic hydrogen generation, Chem. Rev. 110 (2010) 6503–6570.
[4] J. Qi, W. Zhang, R. Cao, Solar-to-hydrogen energy conversion based on water splitting, Adv. Energy Mater. 8 (2018) 1701620.
[5] T. Takata, J. Jiang, Y. Sakata, M. Nakabayashi, N. Shibata, V. Nandal, K. Seki, T. Hisatomi, K. Domen, Photocatalytic water splitting with a quantum efficiency of almost unity, Nature 581 (2020) 411–414.
[6] Y. Zhao, C. Ding, J. Zhu, W. Qin, X. Tao, F. Fan, R. Li, C. Li, A hydrogen farm strategy for scalable solar hydrogen production with particulate photocatalysts, Angew. Chem. Int. Ed. 59 (2020) 9653–9658.
[7] Z. Zou, J. Ye, K. Sayama, H. Arakawa, Direct splitting of water under visible light irradiation with an oxide semiconductor photocatalyst, Nature 414 (2001) 625–627.
[8] T. Hisatomi, J. Kubota, K. Domen, Recent advances in semiconductors for photocatalytic and photoelectrochemical water splitting, Chem. Soc. Rev. 43 (2014) 7520–7535.
[9] T. Hisatomi, K. Domen, Reaction systems for solar hydrogen production via water splitting with particulate semiconductor photocatalysts, Nat. Catalysis 2 (2019) 387–399.
[10] J. Zhang, W. Yao, C. Huang, High efficiency and stable tungsten phosphide cocatalysts for photocatalytic hydrogen production, J. Mater. Chem. A 5 (2017) 12513–12519.
[11] Y. Shen, D. Li, Y. Dang, J. Zhang, W. Wang, B. Ma, A ternary calabash model photocatalyst (Pd/MoP)/CdS for enhancing H_2 evolution under visible light irradiation, Appl. Surf. Sci. 564 (2021), 150432.
[12] J. Zhang, Y. Dang, W. Wang, H. Zhan, X. Song, B. Ma, Efficiently improving the photocatalytic hydrogen evolution of g-C_3N_4 by (Pt/MoP) composite co-catalyst with low amount of Pt, Int. J. Hydrog. Energy 47 (2022) 2338–2346.
[13] B. Ma, H. Xu, K. Lin, J. Li, H. Zhan, W. Liu, C. Li, Mo_2C as non-noble metal co-catalyst in Mo_2C/CdS composite for enhanced photocatalytic H_2 evolution under visible light irradiation, ChemSusChem 9 (2016) 820–824.
[14] L. Luo, D. Li, Y. Dang, W. Wang, G. Yu, J. Li, B. Ma, Capacitance catalysis: positive and negative effects of capacitance of Mo_2C in photocatalytic H_2 evolution, ACS Sustain. Chem. Eng. 10 (2022) 5949–5957.
[15] Y. Dang, L. Feng, W. Hu, W. Wang, Q. Zhang, B. Ma, A 3D flower-like WC with large capacitance as efficient co-catalyst in photocatalytic H_2 evolution, Int. J. Hydrog. Energy 46 (2021) 39251–39261.
[16] J. Sun, L. Duan, Q. Wu, W. Yao, Synthesis of MoS_2 quantum dots cocatalysts and their efficient photocatalytic performance for hydrogen evolution, Chem. Eng. J. 332 (2018) 449–455.
[17] M. Wang, J. Cheng, X. Wang, X. Hong, J. Fan, H. Yu, Sulfur-mediated photodeposition synthesis of NiS cocatalyst for boosting H2-evolution performance of g-C_3N_4 photocatalyst, Chin. J. Catal. 42 (2021) 37–45.
[18] B. Ma, Y. Dang, D. Li, X. Wang, K. Lin, W. Wang, X. Zhou, Y. Chen, T. Xie, X. Zhang, H. Han, A Yin-Yang hybrid co-catalyst (CoO_x-Mo_2N) for photocatalytic overall water splitting, Appl. Catal. B Environ. 298 (2021), 120491.
[19] B. Ma, X. Li, D. Li, K. Lin, A difunctional photocatalytic H_2 evolution composite co-catalyst tailored by integration with earth-abundant material and ultralow amount of noble metal, Appl. Catal. B Environ. 256 (2019), 117865.
[20] K. Lin, L. Feng, D. Li, J. Zhang, W. Wang, B. Ma, Improved photocatalytic hydrogen evolution on (Ru/WC)/CdS via modulating the transferring paths of photo-excited electrons, Appl. Catal. B Environ. 286 (2021), 119880.
[21] B. Ma, S. Zhang, W. Wang, L. Feng, R. Zhang, K. Lin, D. Li, H. Zhan, X. Yang, A novel earth-abundant W-WC heterojunction as efficient co-catalyst for enhanced photocatalytic H_2 evolution, ChemCatChem 12 (2020) 1148–1155.
[22] M. Ledendecker, S.K. Calderón, C. Papp, H.-P. Steinrück, M. Antonietti, M. Shalom, The synthesis of nanostructured Ni_5P_4 films and their use as a non-noble bifunctional electrocatalyst for full water splitting, Angew. Chem. Int. Ed. 54 (2015) 12361–12365.
[23] T. Zhang, K. Yang, C. Wang, S. Li, Q. Zhang, X. Chang, J. Li, S. Li, S. Jia, J. Wang, L. Fu, Nanometric Ni_5P_4 clusters nested on $NiCo_2O_4$ for efficient hydrogen production via alkaline water electrolysis, Adv. Energy Mater. 8 (2018) 1801690.
[24] Y. Huang, L. Hu, R. Liu, Y. Hu, T. Xiong, W. Qiu, M.-S. (J. Tang) Balogun, A. Pan, Y. Tong, Nitrogen treatment generates tunable nanohybridization of Ni_5P_4 nanosheets with nickel hydr(oxy)oxides for efficient hydrogen production in alkaline, seawater and acidic media, Appl. Catal. B Environ. 251 (2019) 181–194.
[25] X. Liu, Y. Zhao, X. Yang, Q. Liu, X. Yu, Y. Li, H. Tang, T. Zhang, Porous Ni_5P_4 as a promising cocatalyst for boosting the photocatalytic hydrogen evolution reaction performance, Appl. Catal. B Environ. 275 (2020), 119144.
[26] C. Feng, Y. Wang, Z. Lu, Q. Liang, Y. Zhang, Z. Li, S. Xu, Nanoflower Ni_5P_4 coupled with GCNQDs as Schottky junction photocatalyst for the efficient degradation of norfloxacin, Sep. Purif. Technol. 282 (2022), 120107.
[27] L. Bao, J. Zang, X. Li, Flexible Zn_2SnO_4/MnO_2 core/shell nanocable−carbon microfiber hybrid composites for high-performance supercapacitor electrodes, Nano Lett. 11 (2011) 1215–1220.
[28] Y. Zhang, W. Zhou, Y. Tang, Y. Guo, Z. Geng, L. Liu, X. Tan, H. Wang, T. Yu, J. Ye, Unravelling unsaturated edge S in amorphous NiS_x for boosting photocatalytic H_2 evolution of metastable phase CdS confined inside hydrophilic beads, Appl. Catal. B Environ. 305 (2022), 121055.
[29] J. Xu, W. Zhong, D. Gao, X. Wang, P. Wang, H. Yu, Phosphorus-enriched platinum diphosphide nanodots as a highly efficient cocatalyst for photocatalytic H_2 evolution of CdS, Chem. Eng. J. 439 (2022), 135758.
[30] S. Xu, Y. Du, X. Liu, X. Yu, C. Teng, X. Cheng, Y. Chen, Q. Wu, Three-dimensional (3D) hierarchical coral-like Mn-doped Ni_2P-Ni_5P_4/NF catalyst for efficient oxygen evolution, J. Alloy. Compd. 826 (2020), 154210.
[31] J. Lin, C. Wang, S. Wang, Y. Chen, W. He, T. Ze, B. Chen, Preparation of rimose NiZnP electrode for hydrogen evolution reaction in alkaline medium by electroless and H_2SO_4 etching, J. Alloy. Compd. 719 (2017) 376–382.